Reprinted from:

SHOCK WAVES AND HIGH - STRAIN - RATE PHENOMENA IN METALS (1981)
Edited by Marc A. Meyers and Lawrence E. Murr
Book available from: Plenum Publishing Corporation
233 Spring Street, New York, N.Y. 10013

Chapter 27

THE ATTENUATION OF SHOCK WAVES IN NICKEL

Chen-Yih Hsu
Kou-Chang Hsu
Lawrence E. Murr
Marc A. Meyers

Department of Metallurgical and Materials Engineering
New Mexico Institute of Mining and Technology
Socorro, New Mexico U.S.A.

The attenuation of planar shock waves generated by plate impact was monitored by their decay throughout massive nickel blocks. This was accomplished, during the passage of the wave, by manganin piezoresistive gages connected to oscilloscopes and, in the post-shocked condition, by hardness measurements and TEM observations at various distances from the impact surface in the nickel blocks. The nickel systems exhibited different metallurgical microstructures before shock loading: preshocked (grain size 150 μm), annealed (grain size 150 μm), and annealed (grain size 32 μm). For each system, two different initial shock pressures were used: 10 and 25 GPa. The pulse duration was held constant at 2 μs. The experimental records of oscilloscopes showed that there are no significant effects of grain size and pre-deformation on the attenuation in nickel. The observed attenuation was compared with the calculated one according to hydrodynamic theory and poor agreement was found. An "accumulation" model based on the conservation of energy is presented herein to explain the dissipative processes of shock waves in metals.

I. INTRODUCTION.

The parameters that affect the shock loading response of metals and alloys may be divided into two categories: (a) material parameters and (b) shock-wave parameters. Numerous studies have been conducted on the effects of shock-wave pressure and pulse duration (1-5), but the attenuation has only received a limited

attention, and the understanding of metallurgical effects upon the attenuation of shock waves is lacking.

The objectives of this investigation were to determine whether metallurgical parameters have a noticeable effect on the attenuation rate in nickel; the grain size and dislocation substructure were chosen as parameters. The attenuation of shock waves having initial amplitudes of 10 and 25 GPa with pulse duration of 2 μs was monitored by their decay throughout six nickel systems with different grain sizes and degrees of pre-strain. This was accomplished by manganin gages connected to oscilloscopes during the events, and post-shocked hardness measurements, as well as electron optical observation at various positions within the nickel blocks.

II. EXPERIMENTAL MATERIALS AND PROCEDURE

A. Materials System

One-inch thick plates of commercial nickel 200 (99.5 pct pure) were used for the systems. The pre-deformation and different grain sizes were obtained as follows.
(a) Pre-Shocked: the as-received nickel plates were annealed *in vacuo* at 1478° K/5 hours; the resulting grain size as determined from the linear intercept method was 150 μm. Following this step, both top and bottom surfaces of each plate were shocked sequentially by contact explosives (6); an explosive layer consisting of one Detasheet C-1 and one Detasheet C-2 (3 mm total) was used for each event. The Detasheet (pressure vs. particle velocity) intersects the Ni curve at a pressure of 33 GPa (6). One obtains a pressure of about 14 GPa by introducing the correction factor of 0.42 (7) for grazing incidence of the detonation; the pulse duration is zero.
(b) Large-grain size (annealed): the as-received nickel plates were annealed at 1478°K/5 hours *in vacuo* for obtaining the large grain size (150 μm).
(c) Small-grain size (annealed): the as-received nickel plates were cold rolled to a 30 pct reduction in thickness and then annealed at 988°K/55 min. for obtaining small grain size (32 μm).

The nickel systems used in the experiment were slightly different from the ones commonly used in shock-wave studies. They are schematically shown in Figure 1. All faces and sides of each nickel plate were milled to assure a good fit and exact dimensions of 15 cm x 15 cm. The nickel plates were stacked up and bolted together at two corners. They were packed with vaseline to avoid air pockets and unwanted reflections. The nickel blocks were laterally protected by spall rails (stainless steel). A spall plate in the bottom was used for the trapping of the reflected

tensile waves. The gages were embedded between gage plates and kept at the same distance (10.4 cm) for each system. The pre-shocked and large-grain systems consisted of eight nickel plates while the small-grain systems consisted of twelve nickel plates.

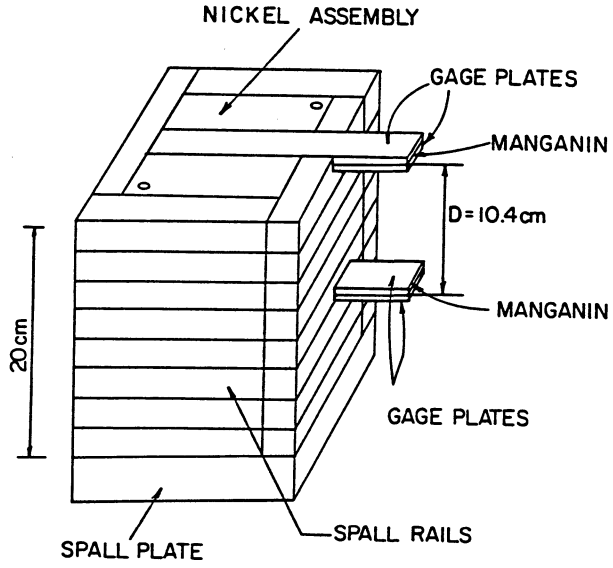

FIGURE 1. Schematic arrangement of nickel systems.

The explosive used in the experiment was "Detasheet C", a DuPont PETN-base plastic explosive with density of 1.45 g/cm^3. The detonation velocity is 7200 m/s. One can calculate the driver-plate thicknesses and required explosive loads at 10 and 25 GPa with pulse duration of 2 μs by following the methods described by Orava and Wittman (6) and De Carli and Meyers (8). Table I shows the experimental conditions for the six events.

B. Experimental Techniques.

The parallel-plate and inclined-plate assemblies were used for the 25 GPa and 10 GPa events, respectively. The sliced-cone geodesic line-initiator was used as line-wave generator. The experimental assemblies are shown in Figure 2. During the events, the measurement of pressure at the same position for each system was accomplished by means of manganin gages. Their characteristics were: four terminals, π shaped, 50 μΩ resistance. They were manufactured by Mr. T. Gano of S^2. Each transducer gage was connected to oscilloscopes. The primary oscilloscope was connected to the EDU (Explosive Detonating Unit) and triggered with pre-calculated time delays of 50 μs (top osc.) and 75 μs (bottom osc.). The secondary oscilloscope was connected to a pin and

TABLE I. Experimental Conditions for Systems (Initial pulse duration: 2μs)

Systems	Grain Size (μm)	Pressure (GPa)	Driver Plate (Ni) Thickness (mm)	No. of Explosive Layers Required (Detasheet C-1)
1. Preshocked	150	10	5.07	8
2. Annealed (L.G.S.)[a]	150	10	5.07	8
3. Annealed (S.G.S.)[b]	32	10	5.07	8
4. Preshocked	150	25	5.45	18
5. Annealed (L.G.S.)[a]	150	25	5.45	18
6. Annealed (S.G.S.)[b]	32	25	5.45	18

[a] L.G.S.: Large Grain Size

[b] S.G.S.: Small Grain Size

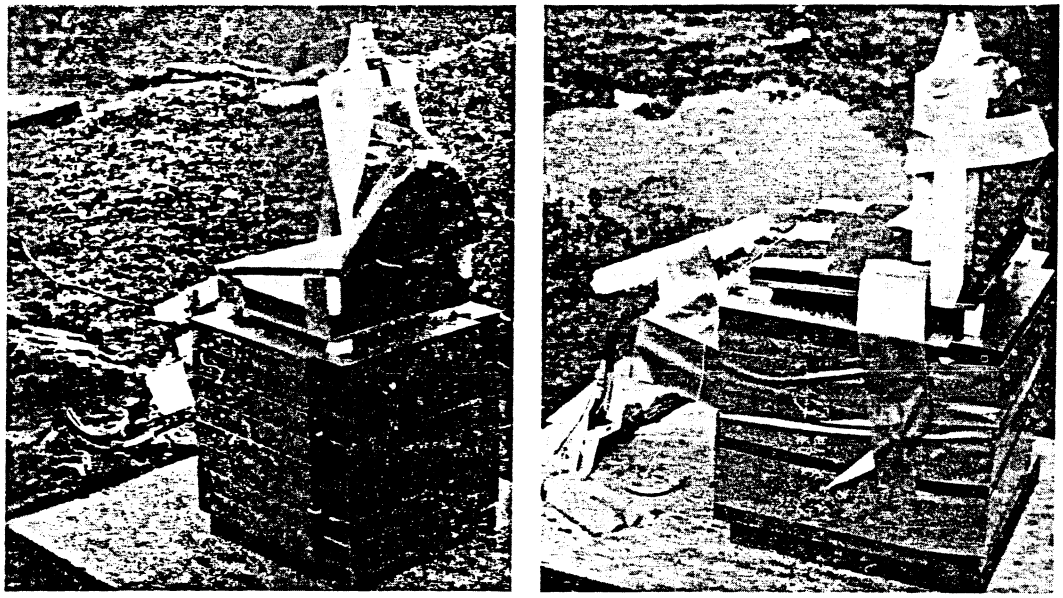

(a) *(b)*

FIGURE 2. Experimental assemblies: (a) Parallel-plate; 25 GPa, 2 μs. (b) Inclined-plate; 10 GPa, 2 μs.

triggered with a precalculated time delay of 5 μs (top osc.) and 25 μs (bottom osc.). They were set up to record the signal (voltage) induced in the transducer by the application of a source of constant current to the transducer and its change due to the change in resistance of the manganin wire as it was compressed. The pressure-monitoring arrangement for each shot required four oscilloscopes; this is illustrated in Figure 3.

As the shock front reached the top and bottom gages, the change of resistance of manganin wire (ΔR) was recorded in the film. The pressure can be calculated by applying the following two empirical equations:

$$P = 35 \left(\frac{\Delta R}{R_o} \right) \text{ GPa} \qquad [1]$$

$$P = 48 \left(\frac{\Delta R}{R_o} \right) - 5.6 \text{ GPa} \qquad [2]$$

Equation [1] applies for pressures between 2 and 15 GPa and equation [2] for pressures higher than 15 GPa. A very rough measure of the attenuation rate can be obtained by dividing the pressure difference between two gages by the travel distance (10.4 cm). Representative oscilloscopic records are shown in Figure 4.

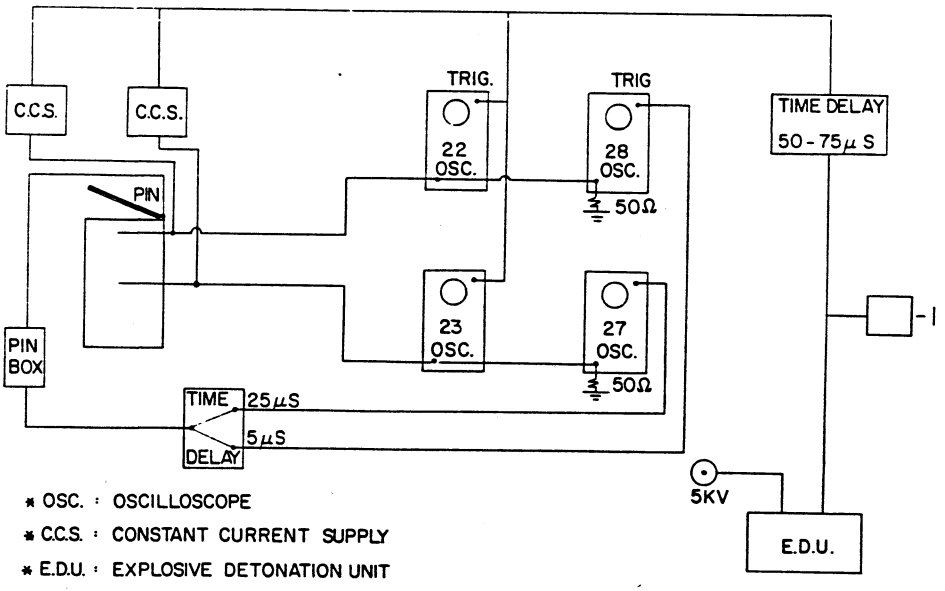

FIGURE 3. The pressure monitoring arrangement of each shot.

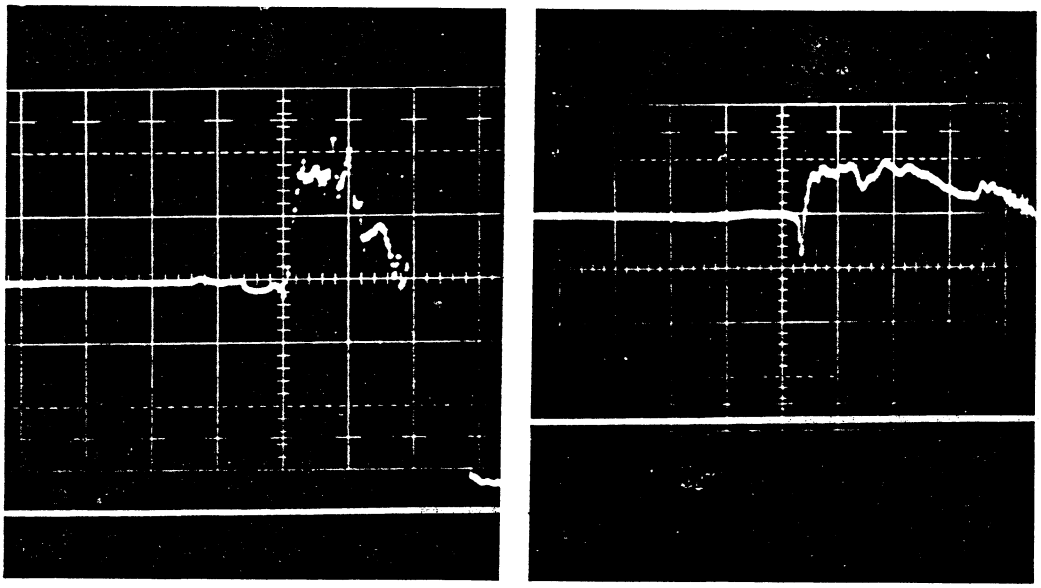

(a) *(b)*

FIGURE 4. Representative oscilloscope records of event 5, 25 GPa. (a) Secondary oscilloscope of top gage. 5 μs delay window-20 μs; (b) Secondary oscilloscope of bottom gage, 25 μs delay, window-20 μs.

Before conducting shock-wave deformation, the hardnesses were measured on the top, bottom and lateral surfaces of each plate. After shock loading, the hardness measurements were conducted in the same way on the central part of shocked plate, after each plate was sawed.

The T.E.M. specimens were taken from the central part of shocked plates at positions of 1, 9, and 18 cm from the top surface of each system. The nickel in the pre and post-shocked condition was cut into 0.3 mm-thick sheets parallel to the surface of the plate by using a Buehler Isomet low-speed saw. Following this step, electrothinning with a solution of 50 pct. H_3PO_4, 30 pct. H_2SO_4, and 20 pct. H_2O at 7 V (at a current density of 1.5-2.0 amp/cm^2) was used until 0.1 mm-thick. The thinned samples were punched into 3 mm disks and electropolished at 50 mA with the above-named electrolyte in a Fishione Twin-jet electropolisher. Then they were examined in a HITACHI PERKIN-ELMER HU 200 F transmission electron microscope operated at 200 KV. The grid intercept method described by Keh (9) was used to measure dislocation density. An average film thickness of 3200 A was used in all dislocation density measurements.[1] The mean dislocation cell size was determined by the linear intercept technique.

III. RESULTS AND DISCUSSION

Figure 4 shows the representative oscilloscope records of the manganin gage. The comparison of the calculated results and experimental results is shown in Table II. One can see that the differences between the calculated and measured pressure are about 5 pct. for the 10 GPa events and 10 pct. for the 25 GPa events; hence, the pressures predicted by the Gurney-Hugoniot treatment are in fair agreement with the measured values. The measured rarefaction rates are lower than the calculated values. The measured attenuation rate at 25 GPa is higher than at 10 GPa. One can also observe that there is no significant difference in attenuation rate between large-grain size, small-grain size, and preshocked systems at 25 GPa. Thus one can say that the existing dislocation substructure and grain size have little effect on the attenuation of shock waves in nickel. The attenuation of a planar shock wave produced in a solid by a flyer plate can be predicted by neglecting dissipative processes and effects of material rigidity (10); this calculation is based on the hydrodynamic theory. The predicted profiles are shown in Figure 5 along with experimental values at 1 and 10 cm from the impact surface. The calculations are straightforward and the pulse profiles at various distances from the impact surface are determined by computing the velocities of the shock front and rarefaction part of the wave (at four different pressures);

[1] *The average foil thickness was determined from projection width measurements and extinction fringe measurements.*

TABLE II. Comparison of Results of Calculation and Measurement from Oscilloscope Records.

System	Pre-Shocked	Large grain size	Small grain size	Pre-Shocked	Large grain size	Small grain size
Calculated Pressure (GPa)	10	10	10	25	25	25
Calculated Pulse Duration (μs)	2	2	2	2	2	2
Calculated Rarefaction Rate (GPa/μs)	70.8	70.8	70.8	83.7	83.7	83.7
Measured Pressure on Top gage (GPa)	9.6	9.5	9.8	[a]	22.9	22.6
Measured Pressure on Bottom gage (GPa)	[a]	4.8	[a]	14.7	13.1	11.7
Measured Pulse Duration (μs)	~1.1	[a]	~1.1	[a]	~1.2	~1.4
Measured Attenuation Rate (GPa/cm)	[a]	0.5	[a]	0.8[b]	0.9	1.0
Measured Rarefaction Rate (GPa/μs)	19.2	[a]	[a]	[a]	35.8	34.5

[a]: The transducer gages were broken during the events.

[b]: Calculated assuming pressure of 22.8 GPa on top gage.

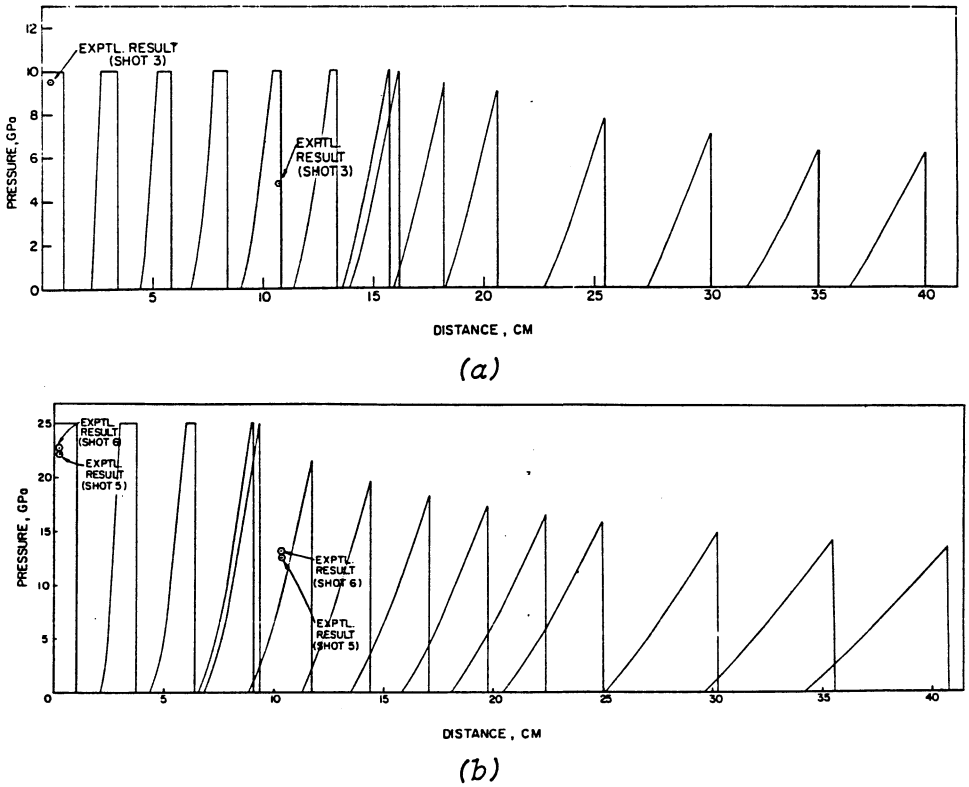

FIGURE 5. Comparison of attenuation predicted by hydrodynamic model and experimental results (a) 10 GPa (b) 25 GPa

the release wave steadily overcomes the shock front because of its higher velocity. The procedure is illustrated in Figures 1 and 2 of Orava and Wittman (6). The measured decay rate of the pulse is much higher than the one predicted from the hydrodynamic theory. Hence, the hydrodynamic theory does not realistically depict the attenuation of shock waves and alternative approaches should be pursued. This will be discussed later in this section. Similar results were found by Erkman and Christensen (11) in aluminum, their measured attenuation rates were much lower than the predictions from the hydrodynamic theory.

Figure 6 shows the hardness results prior to and after shocking at 10 and 25 GPa peak pressure. As expected, the hardness decreases as shock wave itself travels downward in trajectory. The hardness readings near the top surface of the annealed nickel blocks are consistent with the results of Trueb (12). Figure 6 reveals that the hardness increases in annealed systems were much greater than in preshocked systems. The hardness profiles for large and small grain size systems are similar. This is consistent with the manganin gage results. For preshocked systems, the hardness changes were much smaller. Each plate had previously

been shot twice at about 14 GPa pressure and there is no apparent hardness increase 10 cm below the impact surface for the 10 GPa event and 15 cm below it for the 25 GPa event.

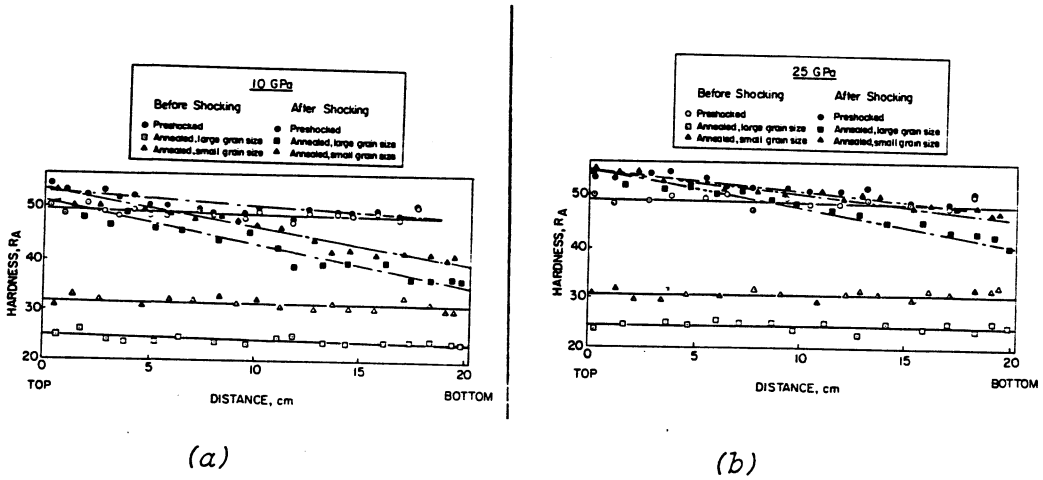

(a) *(b)*

FIGURE 6. Comparison of hardness profiles for six nickel systems. (a) 10 GPa (b) 25 GPa

Figures 7-12 show the residual microstructures of shocked nickel systems at the positions of 1, 9, and 18 cm from the top surface. As expected, no twinning or phase transformation was found in the residual microstructures: a dislocation cell structure was produced. The mean dislocation cell sizes of shocked nickel systems are summarized in Table III. It is shown that there is no apparent difference in dislocation cell size between large grain size and small grain size systems, at both 10 and 25 GPa. The dislocation-cell size increases from top surface to the bottom; the dislocation-cell size increases as pulse pressure decreases. For preshocked systems, the dislocation-cell sizes increase as pulse pressure decreases. For preshocked systems, the dislocation-cell sizes decrease due to repeated shocking.

Table IV summarizes the dislocation densities. The dislocation densities of shocked nickel are consistent with the previous work of Murr *et al.* (13). On examining Table IV, it is observed that the dislocation densities decline from the top surface to the bottom. The decrease is in good agreement with the hardness results. There is some dislocation density increase for preshocked systems. This is consistent with recent work of Kazmi and Murr (14), who investigated the residual microstructure of stainless

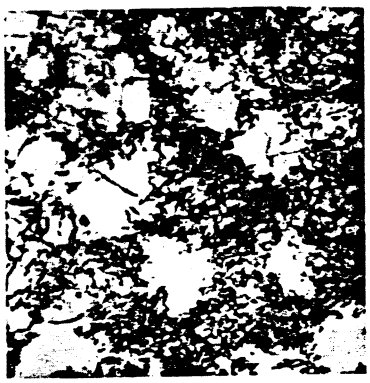

A

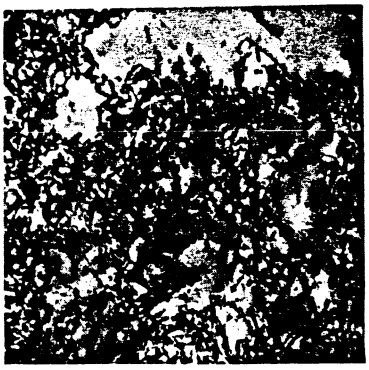

B

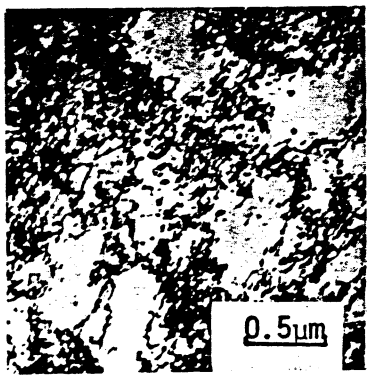

C

FIGURE 7. Transmission electron micrograph of preshocked system shocked at 10 GPa: (a) 1 cm, (b) 9 cm, (c) 18 cm from top surface.

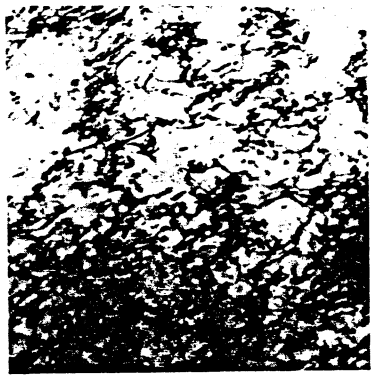

A

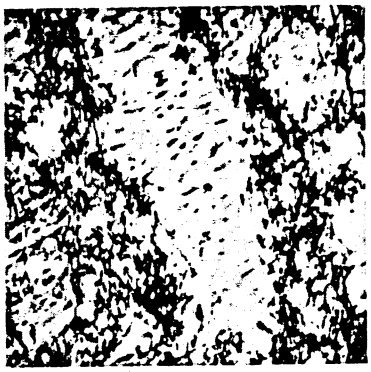

B

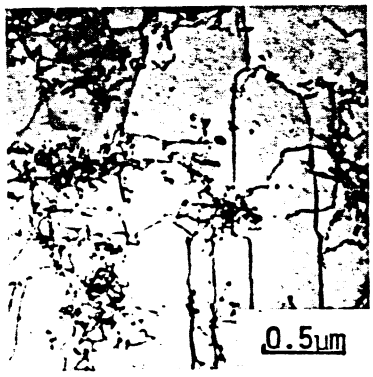

C

FIGURE 8. Transmission electron micrographs of annealed large grain size system shocked at 10 GPa: (a) 1 cm, (b) 9 cm, (c) 18 cm from top surface.

FIGURE 9. Transmission electron micrographs, of annealed small grain size system, shocked at 10 GPa (a) 1 cm, (b) 9 cm, (c) 18 cm from top surface.

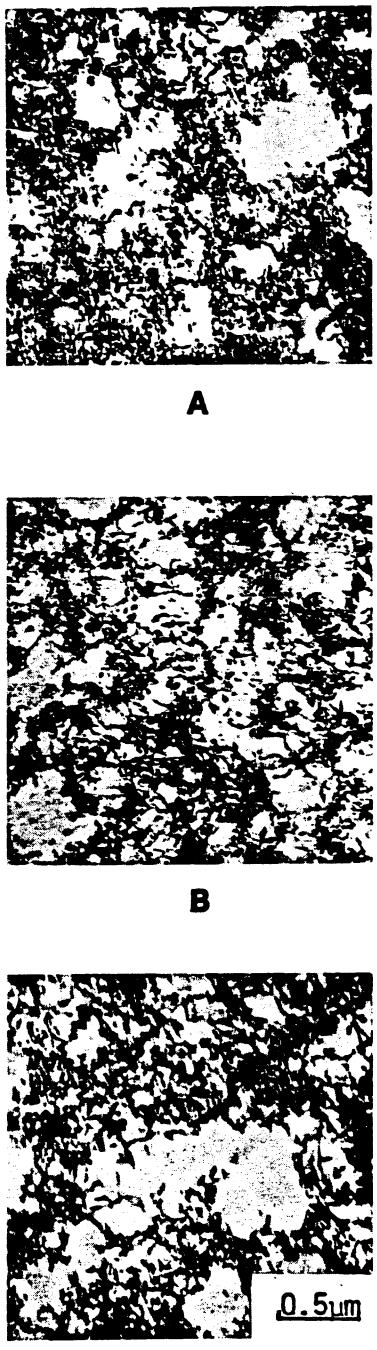

FIGURE 10. Transmission electron micrographs of preshocked system shocked at 25 GPa (a) 1 cm, (b) 9 cm, (c) 18 cm from top surface.

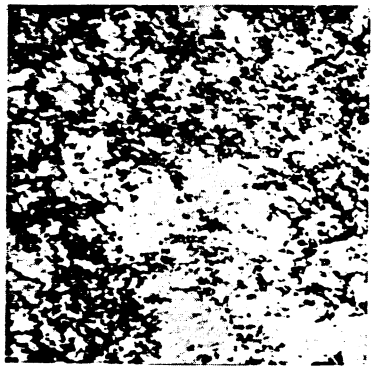

A

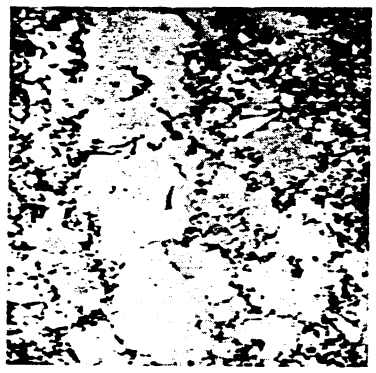

B

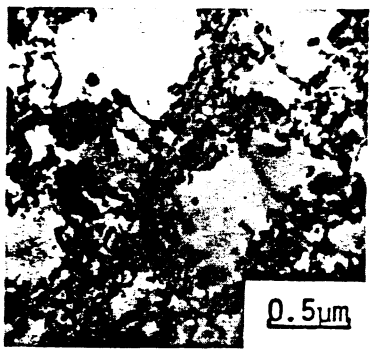

C

FIGURE 11. Transmission electron micrographs of annealed large grain size system shocked at 25 GPa (a) 1 cm, (b) 9 cm, (c) 18 cm from top surface.

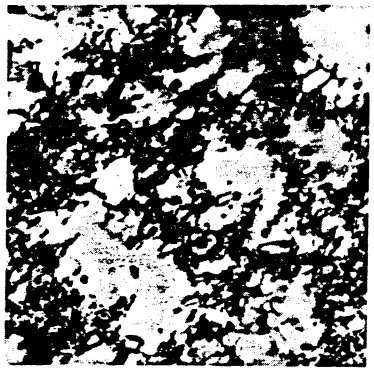

A

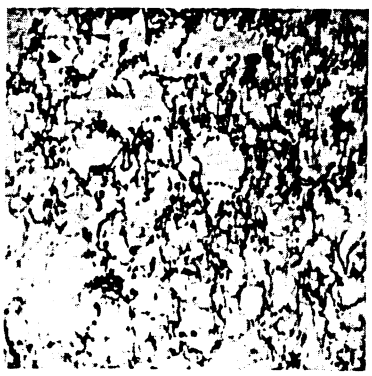

B

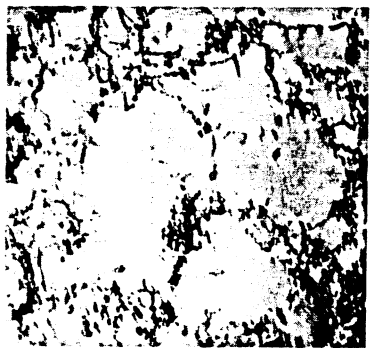

C

FIGURE 12. Transmission electron micrographs of annealed small grain size system shocked at 25 GPa (a) 1 cm, (b) 9 cm, (c) 18 cm from top surface.

TABLE III. The Mean Dislocation Cell Size of Each System.

Systems	Pressure (GPa)	Dislocation cell size before shocking (μm)	Dislocation cell sizes (μm)		
			1 cm from top	9 cm from top	18 cm from top
1. Preshocked	10	0.55	0.32	0.44	0.53
2. Large-grain size	10		0.56	0.67	a
3. Small-grain size	10		0.64	a	a
4. Preshocked	25	0.55	0.27	0.35	0.45
5. Large-grain size	25		0.29	0.39	0.44
6. Small-grain size	25		0.35	a	a

a Clear cells could not be distinguished.

TABLE IV. Dislocation Density of Six Nickel Systems[a,b]

Systems	Pressure (GPa)	Dislocation Density Before Shocking ($X10^{10}$ cm^{-2})	Dislocation Density After Shocking ($X10^{10}$ cm^{-2})		
			1 cm from top	9 cm from top	18 cm from top
Preshocked	10	2.7	5.5	3.5	2.9
Large-Grain Size	10		2.7	1.4	1.0
Small-Grain Size	10	0.17	3.1	1.7	1.2
Preshocked	25	2.7	6.9	5.5	4.0
Large-Grain Size	25		5.0	3.9	2.0
Small-Grain Size	25	0.17	5.6	3.9	2.4

[a]The pulse duration of each shot was 2 μs.

[b]Dislocation densities have been corrected by considering the operating reflection and compensating for the out-of-contrast fraction according to Table 17.1, P. 423 of Hirsch, et al., "Electron Microscopy of Thin Crystals", Butterworth, London, 1969.

steel subjected to shock at 15 GPa pressure and found that dislocation densities were increased even after subjected to three shock pulses. However, one can see that the increases of residual dislocation density in preshocked systems are much lower than in annealed systems at both 10 and 25 GPa shot conditions. Meyers (15) recently proposed a model of dislocation generation in shock loading and mentioned that dislocations are homogeneously generated at the shock front. He also pointed out that if a pre-strained metal is shock-loaded, part of the deviatoric stresses at the shock front could be accommodated by the existing dislocations; in this case the number of dislocations that would be generated at the front would be reduced. These experimental results seem to corroborate this idea. Since the hydrodynamic theory does not satisfactorily predict the attenuation of shock waves, it was modified mathematically by a method introduced by Von Neumann and Richtmyer (16) in which an artificial viscosity was used to smooth discontinuities in the flow. This modified method predicts more realistic decays but does not have a clear physical meaning.

In this report, an attempt is made to explain physically the dissipative mechanisms responsible for the attenuation of the pulse. This model is named "accumulation model" because it is based on the conservation-of-energy law:

INPUT - OUTPUT = ACCUMULATION

The following calculation provides a further understanding. Assume that a shock wave with a peak pressure of 10 GPa and 2 μs pulse duration travels 1 cm through a nickel plate of 1 cm^2 cross-section area. According to the Rankine-Hugoniot theory, shown in Figure 5, one can calculate internal energy per unit volume, E. The energy can be expressed as work per unit area. In this case, the energy of the incoming pulse with 2 μs pulse duration is 232.8 J/cm^2. From a viewpoint of metallurgy, point defects, line defects, twinning, precipitates, martensitic transformations, and heating are dissipative processes causing the attenuation of a shock wave. Since no twinning, precipitation, or phase transformation occurs in the pressure range of 10 and 25 GPa, point and line defects generation, hydrodynamic residual rise in temperature, and temperature rise due to dislocation motion are the significant mechanisms responsible for the attenuation of shock waves in nickel. Dieter (17) estimated the total strain energy of a dislocation is 1.36×10^{-18} J per atomic plane. The lattice parameter of nickel is 3.52A. By multiplying the dislocation density of 3.1×10^{10} cm/cm^3, the total strain energy of dislocations is 1.2 J/cm^3. The vacancy concentration at 10 GPa is about $3.85 \times 10^5/cm^2$ (18). The formation energy being 1.6×10^{-19} J per vacancy, one obtains 6.2×10^{-14} J/cm^3 for vacancies. This value is so small that it can be neglected. According to the hydrodynamic Rankine-Hugoniot theory, the residual temperature rise is 2 K (8) for nickel at

10 GPa. The heat capacity of nickel is 39 J/Kcm^3. The thermal energy change is 7.8 J/cm^3. The total above accumulation energy is about 9.0 J/cm^3. Subtracting this value from the input, one obtains an output of 223.8 J/cm^2 after shock wave travels 1 cm within nickel plate. Figure 13 shows a comparison of "accumulation model" with the hydrodynamic theory and experimental results.

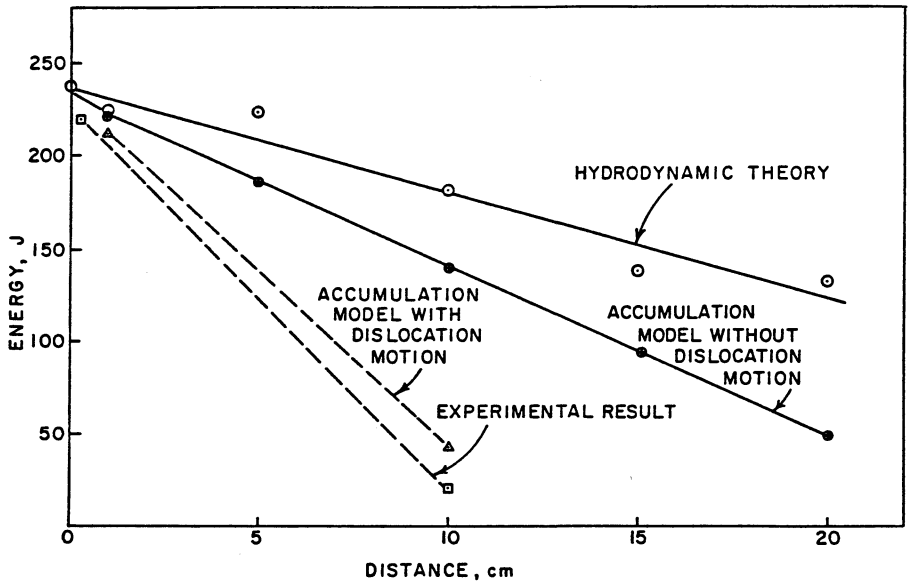

FIGURE 13. Pulse energy in its downward trajectory.

One can see that there is still discrepancy between "accumulation" model and the experimental results. This difference is of about 120 J at a distance of 10 cm from the top, or an average of 12 J/cm. Hence, dislocation motion was introduced into the model to take into account the additional energy dissipation. This can be done by applying Peach-Koehler's equation assuming that the work required to move a dislocation is totally converted into heat:

$$W = \tau b l \rho$$

where τ is the applied shear stress, b is the Burgers vector (3.5 x10^{-10} m), l is the distance moved by each dislocation, ρ the dislocation density. Setting this work equal to 12 J and assuming, to a first approximation, that each dislocation moves 0.7 μm. One can compute τ; ρ is about 3.1x10^{10} cm^{-2} (Table III). One finds that τ is approximately 0.16 GPa. From the stress vs. velocity plot presented by Meyers (Figure 4 of ref. 21) for nickel, one can estimate the velocity at which the dislocations would have to move to dissipate the required amount of energy (12 J/cm); it is around

V. ACKNOWLEDGMENT

The first series of explosive events was conducted at Ellsworth Air Force Base and Sgt. Poundstone provided valuable help. A special gratitude is extended to Mr. P.S. De Carli for the planning and execution of the final explosive events and to Mr. L.B. Hall for the instrumentation.

The authors gratefully acknowledge the financial support of the National Science Foundation Grant Number DMR-792102.

VI. REFERENCES

1. Appleton, A.S., and Waddington, J.S., *Acta Met.*, 12, 956 (1964).
2. Champion, A.R., and Rohde, R.W., *J. Appl. Phys.*, 41, 2213 (1970).
3. Lokken, R.O., Stone, G.A., and Orava, R.N., South Dakota School of Mines and Technology, unpublished results.
4. Murr, L.E., and Huang, J.Y., *Materials Science and Engineering*, 19, 115 (1975).
5. Moin, E., and Murr, L.E., *Materials Science and Engineering*, 37, 249 (1979).
6. Orava, R.N., and Wittman, R.H., "Proc. 5th International Conf. High Energy Rate Fabrication". U. of Denver, Denver, Colo., P. 111 (1975).
7. Jones, O.E., "Metal Response Under Explosive Loading", in proc. of Behavior and Utilization of Explosive in Engineering Design, L. Davidson et al., (eds.), New Mexico Section, ASME, Albuquerque, N.M., P. 125 (1972).
8. Appendices A-G, this volume.
9. Keh, A.S., "Direct Observation of Imperfections in Crystals", Newkirk, J.B., and Wenick. J.H., (eds.), Interscience Publisher, New York, P. 213 (1962).
10. Fowles, G.R., *J. Appl. Phys.*, 31, 655 (1960).
11. Erkman, J.O., and Christensen, A.B., *J. Appl. Phys.*, 38, 5395 (1970).
12. Trueb, L.F., *J. Appl. Phys.*, 40, 2976 (1969).
13. Murr, L.E., Vydyanath, H.R., and Foltz, J.V., *Met. Trans.* 1, 3215 (1970).
14. Kazmi, B., and Murr, L.E., this volume.(Chapter 41)
15. Meyers, M.A., *Scripta Met.*, 12, 21 (1978).
16. Neumann, J.V. and Richtmyer, R.D., *J. Appl. Phys.*, 21, 232 (1950).
17. Dieter, G.E., "Mechanical Metallurgy", McGraw-Hill Inc., New York, p. 169 (1976).
18. Kressel, H., and Brown, N.J., *J. Appl. Phys.*, 38, 1618 (1967).
19. Buckel, W., and Hilsch, R., *Phys.* 138, 109 (1954).
20. Paneth, H., *Phys. Rev.*, 80, 708 (1950).

500 m/s. This is clearly a subsonic and reasonable value. Hence, the "accumulation model" with dislocation motion shows a reasonable agreement with the experimentally determined attenuation of the shock pulse.

The reason the gages and specimens were from the central part of the nickel blocks is that there are rarefactions initiating at the lateral boundaries during the progression of the shock wave. These rarefactions cause both a rapid stress release and a transition to triaxial strain. Only the central part of the nickel blocks undergo really uniaxial strain; after about 10 cm from the top, the release waves propagate throughout the whole width of the blocks (22).

IV. CONCLUSIONS

(a) The measured attenuation rate is greater than the value predicted by the hydrodynamic theory. It is suggested that the dissipative processes deserve significant consideration in the prediction of attenuation of shock waves in metals.

(b) From the manganin gage results, it is observed that grain size and dislocation substructure do not play an important role in the attenuation of shock waves in nickel.

(c) As expected, the hardness profiles of shocked systems show a decline from top plate to bottom plate consistent with dislocation density results.

(d) The increase of dislocation density, as observed by transmission electron microscopy in preshocked systems, is smaller than in annealed systems. It can be said that part of the deviatoric stresses at the shock front could be accomodated by the existing dislocations in the pre-shocked systems.

(e) An "accumulation model" is presented based on dissipative mechanisms of pulse attenuation: point and line defect generation, temperature rises due to thermodynamic irreversibility in the hydrodynamic theory and due to dislocation motion. It is shown that heating due to dislocation motion is an important energy dissipation mechanism.

21. Meyers, M.A., in "Strength of Metals and Alloys," Vol. I, (eds.), Haasen, P., Gerold, V., and Kostorz, G., Pergamon Press, New York, p. 549 (1979).
22. DeCarli, P.S. and Meyers, M.A., "Design and Instrumentation of Uniaxial Strain Shock Recovery Experiments", this volume, (Chapter 22).